

LETTER TO THE EDITOR

AstroSat/UVIT Study of NGC 663: first detection of Be+sdOB systems in a young star cluster

Sneha Nedhath^{1,2,3*}, Sharmila Rani^{1,4}, Annapurni Subramaniam³, and Elena Pancino¹

¹ INAF — Osservatorio Astrofisico di Arcetri, Largo E. Fermi 5, I-50125 Firenze, Italy

² Dipartimento di Fisica e Astronomia, Università di Firenze, Via G. Sansone 1, I-50019 Sesto Fiorentino (Firenze), Italy

³ Indian Institute of Astrophysics, Koramangala, Bangalore 560034, India

⁴ Aryabhata Research Institute of Observational Sciences (ARIES), Manora Peak, Nainital 263002, India

ABSTRACT

Context. Be stars are rapidly rotating stars surrounded by a disc; however, the origin of these remains unclear. Mass and angular momentum transfer in close binaries account for the rapid rotation of a major fraction of Be stars, supported by the previous detection of low-mass stripped companions to them. The stripped companions can be helium burning subdwarf OB-type stars (sdOBs), and white dwarfs (WDs).

Aims. The main objective of this study is to characterise the identified Be stars in the young open cluster NGC 663, and search for possible hot companions.

Methods. We present the first ultraviolet (UV) photometric study of NGC 663 using far-UV (FUV) and near-UV (NUV) data from UVIT/AstroSat as a part of the UOCS series (XVIII). We identified 23 previously known Be stars in the cluster. Further, we utilised the spectral energy distribution (SED) fitting technique to derive the fundamental parameters and to search for UV-bright companions of the identified Be stars.

Results. Our study reveals that 19 out of 23 Be stars show a significant UV excess, indicating the presence of hot companions. Here, we report the first detection of high-mass sdOB companions to Be stars, with 69.5% of them found in binaries within a cluster, offering direct evidence of binary interactions.

Conclusions. This study showcases the key role of binary interactions in the formation of Be stars in clusters and provides insights into massive star evolution.

Key words. open clusters and associations: individual: NGC 663 – stars: emission-line, Be – binaries: general

1. Introduction

Classical B emission-line stars (Be stars hereafter) are rapidly rotating main-sequence B-type stars surrounded by ionised, gaseous disks. The exact mechanism behind the formation of these disks, commonly known as the "Be phenomenon", remains elusive. Various mechanisms have been proposed to explain how the material is expelled from the Be star into the disk, including rotation, non-radial pulsation, magnetic fields, and the presence of binary companions (Rivinius et al. 2013; Bodensteiner et al. 2020; Mathew et al. 2008).

Binary formation pathway suggests the crucial role of a companion star that fills its Roche lobe, leading to the formation of a circumstellar disk around the Be star. Based on simulations of binary star populations, de Mink et al. (2013) suggested that rapidly rotating massive stars could be spun up either through mass transfer or mergers. Additionally, de Mink et al. (2014) concluded that approximately 30% of all main-sequence (MS) B-type stars are products of dynamical interactions happening among the stars in clusters. Binary population synthesis studies specific to Be stars (Pols et al. 1991; van Bever & Vanbeveren 1997; Shao & Li 2014, 2021) also suggest that at least a significant fraction, if not all, are likely the products of binary interactions.

A series of studies conducted by Peters et al. (2008, 2013, 2016), also support the existence of invisible companions that play a role in the formation of disks in Be stars. Hot companions of these stars are faint in optical and IR, but easily detectable in the far-ultraviolet (FUV) as they emit most of their flux at short wavelengths. Recently, Wang et al. (2021) increased the sample of known Be+sdO binaries.

The majority of the Be-companions are hot subluminal stars of subdwarf O, B type (sdOB) stars (Klement et al. 2022). These companions can subsequently evolve into white dwarfs (WDs) or neutron stars (NSs), potentially leading to the formation of Be/X-ray binaries (BeXBs). Some of these post-mass-transfer (post-MT) systems have already been identified as Be-NS or Be-WD systems, through X-ray outbursts. To detect stripped stars next to an optically bright companion, Götzberg et al. (2018) recommended systematic searches for their UV excess. This clearly showcases the importance and need of employing UV imaging to throw more light on their binary formation pathway. So far, no Be+sdOB systems have been detected in star clusters.

Young open clusters (OCs) with an age of less than a hundred Myr are ideal laboratories for the study of Be stars among the B-type stars and the role of binarity in shaping their properties. In the study by Mathew et al. (2008) covering emission line stars in 42 young OCs, NGC 663 stood out as one of the clusters with

* e-mail: snehanedhath@gmail.com

a large number of Be stars. NGC 663 is a young OC located in the constellation Cassiopeia. Pigulski et al. (2001a) estimated an age of 20-25 Myr and a distance of 2.1 kpc. Recently, Dias et al. (2021) estimated the cluster distance as 2.353 kpc, $\log(t) = 7.403$ yr, $[\text{Fe}/\text{H}] = -0.125$ dex, and $A_V = 2.268$ mag, which are adopted in this work.

This study investigates the ultraviolet properties of Be stars in NGC 663 to check for the presence of hot companions and marks the first detection of binary Be stars with subdwarf companions in OCs, providing evidence of such a formation pathway to Be phenomena in OCs.

2. Data Reduction and Analysis

We used archival data of UVIT onboard *AstroSat* (L1 data from the *AstroSat* data archive¹) and processed them using CCD-LAB Postma & Leahy (2017). A detailed description of UVIT and its calibration can be found in Tandon et al. (2017, 2020). NGC 663 was observed with UVIT on 12th August, 2017 (Proposal Id: A03-079) in three FUV (F148W, F154W, F169M) and two NUV filters (N263M and N279N). CCDLAB corrects for satellite drift, flat field, distortion, fixed pattern noise, and cosmic rays. The orbit-wise images are then co-aligned and merged to get the final science-ready images. Details of the UVIT observations of NGC 663 are tabulated in Table A.1. Figure A.1a shows a composite two-colour image of NGC 663, (F148W (blue) and N279N (yellow)).

3. Photometry

Aperture and Point Spread Function (PSF) photometry are carried out using the DAOPHOT package in IRAF/NOAO Stetson (1987). The model PSF was constructed using bright and isolated stars, then applied to all the detected stars using the ALL-STAR task to get PSF-fitted magnitudes, followed by PSF, aperture, and saturation corrections to obtain the instrumental magnitudes. We note that many bright stars in the cluster were too saturated to derive reliable magnitudes.

The details of the saturation correction are described in (Tandon et al. 2017). Using zero-point (ZP) magnitudes reported in the calibration paper (Tandon et al. 2020), the derived instrumental magnitudes are calibrated into the AB magnitude system. Limiting the PSF fitted error to ~ 0.2 mag (See Figure A.1b in the appendix), stars detected down to ~ 21 mag are selected in F148W, F154W, N236M filters, and down to ~ 19 mag are selected in F169M and N279N filters for further analysis. We use the reddening value of $E(B-V) = 0.7$ mag (Dias et al. 2021), and $R_V = 3.1$ from Whitford (1958) for the Galaxy. As differential extinction within the cluster has been reported by Yadav & Sagar (2001), we use a range in the A_V values with the corresponding extinction in the respective filters tabulated in Table A.1 to overlay the isochrones.

4. Be stars in NGC 663

Sanduleak (1979) found 27 $H\alpha$ emission stars mostly earlier than B5 spectral type, later updated to 24, with 12 stars showing variability in $H\alpha$ emission (Sanduleak 1990). Subsequently, Pigulski et al. (2001b) identified 26 Be stars, with majority between B0 - B3. Later, using the slitless spectroscopy method, Mathew et al.

¹ https://astrobrowse.isdsc.gov.in/astro_archive/archive/Home.jsp

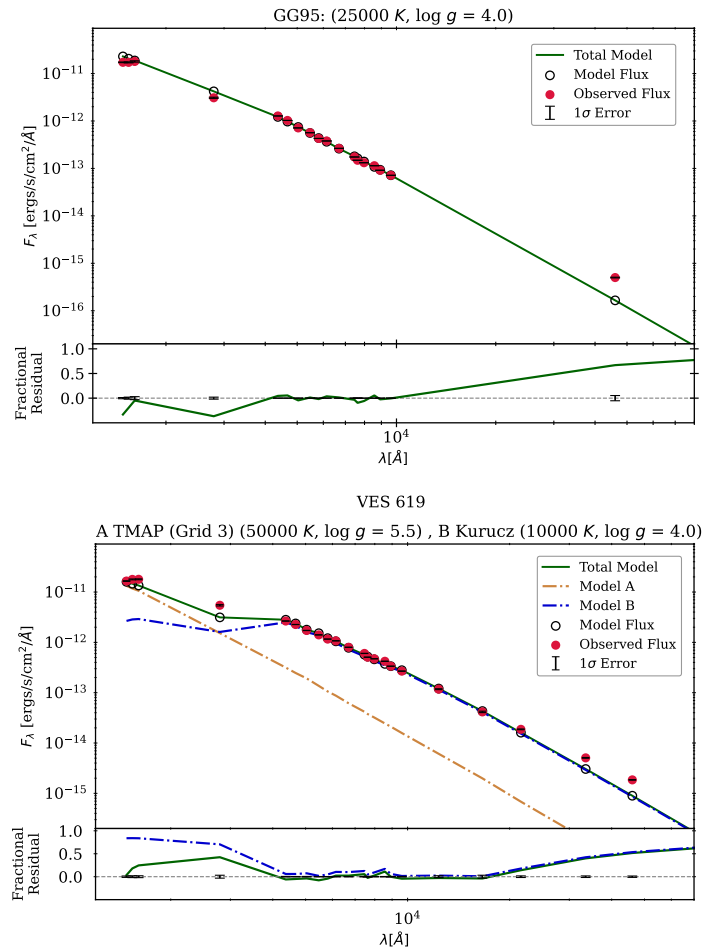


Fig. 1: Upper panel: Single-fit SED of Be star GG 95 with Kurucz model (green line) fitted to observed fluxes (red). Lower panel: SED of Be star VES 619, fitted with a combined Kurucz (blue dash-dotted, cool) and TMAP (brown dash-dotted, hot) model; composite fit shown with a green solid line. Best-fit parameters and model details are shown atop each plot.

(2008) detected several new Be stars, increasing the total count of Be stars in the cluster to 31, in the B0-B8 range. Among the 31 known Be stars, Yu et al. (2015) re-identified 15 stars, and discovered four new Be stars. They concluded that NGC 663 contains a total of 34 Be stars. Of these, 23 stars were detected by UVIT which are analysed in this study.

5. Spectral energy distributions of Be stars

To derive the stellar parameters of the Be stars detected with UVIT, we constructed their spectral energy distributions (SEDs) using the Virtual Observatory SED Analyser (VOSA; Bayo et al. (2008)). Following the construction of the SEDs, best-fit parameters such as T_{eff} , luminosity (L), and radius (R) are derived by performing a reduced chi-square (χ^2_{red}) minimization fitting, which compares the observed fluxes to the synthetic photometric fluxes. The SED fitting technique is described in more detail in Rani et al. (2021). In addition to χ^2_{red} value, VOSA computes two additional parameters, V_{gf} and $V_{\text{gf},b}$, which correspond to modified χ^2_{red} and are used to evaluate the good fit with minimum fractional residual, especially when the observational flux errors

are minimal. For an SED fit to be reliable, the Vgf_b value must be less than 15 (Rebassa-Mansergas et al. 2021). To estimate errors in the derived parameters, VOSA makes use of Markov Chain Monte Carlo (MCMC) approach.

We have used Kurucz stellar atmospheric models (Castelli & Kurucz 2003) to compute synthetic SEDs across a wavelength range extending from FUV to the infrared (IR), encompassing observed photometric data points. These models provide the grid of parameters such as T_{eff} , metallicity ($[Fe/H]$), and surface gravity $\log g$. We fixed metallicity, $[Fe/H]$ of -0.5 dex, close to the cluster metallicity (Paunzen et al. 2010). We adopted a range of $\log g$ values from 3–5 dex, as Be stars span a range of evolutionary phases (Peters 1976) and kept T_{eff} as a free parameter (3,500–50,000 K) in the case of the Kurucz models. We combined three FUV and two NUV UVIT photometric data points with Gaia EDR3 (3 passbands), SLOAN/SDSS (5 passband), 2MASS (3 passbands), and WISE (4 passbands) to construct the observed SEDs. First, we fitted the observed SED, incorporating all the data points, with a single model SED in order to check the overall fitting. Out of 23 stars, 4 stars are well fitted with a single model SED fit, and 19 stars show a significant deviation ($>50\%$) from the model at shorter wavelengths (FUV region). To further confirm the UV excess, we repeated the single model SED fit by excluding the data points with wavelengths less than 3000 Å. After obtaining the stellar parameters, we then employed the VOSA binary fit tool to fit the hotter part of the SED for 19 stars. The VOSA binary fitting tool simultaneously fits the hotter and cooler components of a binary system by assuming that the observed flux is a linear combination of two different models. The Kurucz and TMAP atmospheric models (Rauch & Deetjen 2003) are used to fit the hotter component. The TMAP model grid spans a range of atmospheric parameters, with effective temperatures (T_{eff}) between 50,000 and 190,000 K, surface gravities ($\log g$) between 5 and 9 dex, and a hydrogen mass fraction of zero. For the star GG 101, we were unable to obtain a satisfactory fit using either the Kurucz or TMAP models. Therefore, we adopted the Levenhagen model (Levenhagen et al. 2017), which covers T_{eff} values from 17,000 to 100,000 K and $\log g$ between 7 and 9.5 dex.

Out of 19 stars with UV excess, 16 stars are well fitted with a double-component SED, except three stars, namely, D01 034, GG 109, and SAN 28. We show the best single fit and binary fit SED of Be star GG95 (left panel), and VES 619 (right panel) in Figure 1. The best-fit parameters of 23 Be stars (7 single and 16 binary), derived from the best SED fits with the lowest χ^2_{red} and Vgf_b value are listed in Table B.1. We obtained Vgf_b values below 15 for all of the Be stars, indicating good SED fits and confirming the reliability of all derived fundamental parameters. The remaining best-fit single and double-component SEDs are provided in Appendix B. Since classical Be stars exhibit excess emission in the NUV and IR due to free-bound and free-free processes happening in circumstellar disks, respectively (Goraya 1986), these mechanisms are not efficient at producing significant flux in the FUV regime. Also, note that chromospheric activity cannot account for this UV excess, as B-type stars do not exhibit such activity due to the absence of convective envelopes (Hall 2008). Thus the observed FUV excesses in our sample suggest an additional hot companion. Further, to assess the evolutionary stage and nature of hot companions, we place them in the HR diagram as discussed in the subsequent section.

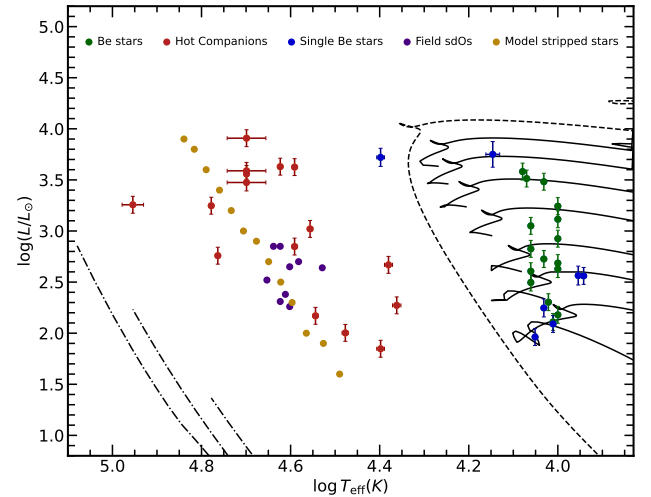


Fig. 2: HR diagram illustrating UVIT-identified Be stars and their hot companions. The cluster isochrone (black dashed), WD evolutionary tracks (black dash-dotted, 0.3–0.5 M_{\odot} , from right to left), and MIST tracks (black solid, 3.0–8.2 M_{\odot} , bottom to top) are shown for comparison. Cool and hot components of binary Be stars are marked in green and brown, and single-fit Be stars are in blue. Field Be+sdO systems from Wang et al. (2021) displayed in purple, and model stripped stars with masses of 0.58, 0.66, 0.74, 0.85, 0.97, 1.11, 1.27, 1.43, 1.63, 1.88, 2.17, 2.49, and 2.87 M_{\odot} from Göteborg et al. (2018) are shown as golden circles (bottom to top).

6. Discussion

This is the first study to trace possible binary companions of Be stars in young clusters. NGC 663 is known to harbour a large number of Be stars for a very long time. These stars also have a large range in spectral type, leading to the inference that the "Be-phenomenon" is operational across the B spectral type in this cluster. Modelling the UV excess and the multi-wavelength SED of 23 Be stars has led to the detection and characterisation of binary companions in 16. The hot companions, as shown in HRD, (Figure 2) belong to the sdOB spectral types and appear to be similar to those found in the field. This study, therefore, provides the first evidence of a binary pathway to Be formation in a young Galactic cluster. NGC 663 has at least 69.5% of Be stars formed through binary mass-transfer, suggesting that a majority of Be stars in NGC 663 are formed via binary mass transfer.

Wang et al. (2021) detected spectral signatures of the sdO companions in 10 of 13 Be stars, and a comparison of their temperatures and radii with evolutionary tracks indicate that the sdO stars occupy the relatively long-lived, He-core burning stage. The companions identified to Be-stars of NGC 663 also occupy a very similar space in the HR diagram (See Figure 17 of Wang et al. (2021)), suggesting these are sdO stars in the long-lived He-core burning phase.

The cluster NGC 663 is 25 Myr old and therefore has a turn-off mass of $\sim 9.2 M_{\odot}$. Recently, (Cavallo et al. 2024) estimated the cluster's age to be 39 Myr, which corresponds to a turn-off mass between ~ 7 –8 M_{\odot} . All the 16 sdOBs are likely to have formed in 25 Myr from a primary star mass of 7–9 M_{\odot} in a binary system. Even though the initial mass is similar, the end mass appears to be different. When we compare the L and T_{eff} of the detected sdOBs with Göteborg et al. (2018) models, we see that the mass of the end products is likely to range be-

tween 0.6 - 2.8 M_{\odot} . The primary stars would have lost different amount of masses during the mass transfer, maybe due to different orbital parameters. The Be stars, the cooler companion of the sdOBs also have a mass range of approximately 2-8 M_{\odot} , which suggests that the Be binaries have a large range for the primary to secondary star mass-ratio. This probably is the reason for the appearance of Be phenomenon across the B-spectral type in this cluster. The dynamical environment of the cluster is also likely to play a role in the binary evolution, as this can alter the binary orbits. As of now, orbital information of these systems are not known, except that many are known to be photometric and/or spectroscopic variables. The binary Be systems in this cluster are therefore very important to investigate binary mass transfer mechanisms in massive stars. The sdOB companions detected here put strong constraints on the mass transfer mechanisms that are crucial to theoretical models such as those presented in Götzberg et al. (2018). The high-resolution spectroscopic studies of the identified Be binary systems in NGC 663 need to be performed to confirm the evolutionary status as well as to explore the atmospheric abundances of the sdOBs. Photometric and spectroscopic variability of these systems also need to be studied systematically to identify orbital parameters. In the future, we plan to extend this study to more young clusters harbouring Be stars.

7. Summary

The main results from this work can be summarised as follows:

- We utilised UVIT/AsrtoSat observations in 3 FUV and 2 NUV filters to characterise 23 Be stars in the young OC NGC 663.
- We estimated atmospheric parameters such as T_{eff} , luminosities, and radii of the Be stars by fitting multiwavelength SEDs with single model spectrum. Among 23 Be stars, 19 exhibited significant UV excess.
- 16 Be stars are well fitted with a double-component SED, indicating the presence of a hot companion. The nature of hot companions is assessed by placing them on the HR diagram and comparing them with the theoretical evolutionary tracks or previously observed field stars of similar class. The position of the detected hot companions coincides with the location of stripped stars (Wang et al. 2021), suggesting that the companions are likely to be stripped stars belonging to the sdOB type in the long-lived He-core burning phase.
- The estimated masses of hot companions range from 0.6 to 2.8 M_{\odot} based on the models of Götzberg et al. (2018), while the Be stars have masses between 2.0 and 8.0 M_{\odot} , derived from the comparison with MIST evolutionary tracks, with many of them slightly evolved from the MS.
- This study establishes the binary pathway to the formation of Be stars in young clusters with 69.5% of Be stars in binary systems in NGC 663. Be binary systems are interesting targets for further high-resolution spectroscopic studies in order to probe their evolutionary status and to gain insights into the abundances of the sdOB stars.

Acknowledgements. We thank the referee for providing the productive report that improved the quality of our manuscript. AS acknowledges support from the SERB Power Fellowship. SN and SR acknowledges support from StarDance: the non-canonical evolution of stars in clusters (co-funded by the European Union, ERC-2022-AdG, Grant Agreement 101093572, PI: E. Pancino). SN also extends gratitude to Blesson Mathew, Sipra Hota, Ashish Devraj, Akhil Krishna and Vikrant Jadhav for the fruitful discussions. This publication utilizes data from the *AstroSat* mission's UVIT, archived at the Indian Space Science Data Centre (ISSDC). The UVIT project is a collaboration between IIA Bengaluru, IUCAA

Pune, TIFR Mumbai, several ISRO centres, and CSA. This research also made use of VOSA, developed under the Spanish Virtual Observatory project, supported by the Spanish MINECO through grant AyA2017-84089.

Software: Topcat (Taylor (2011)), Matplotlib (Hunter (2007)), NumPy (van der Walt et al. (2011)), Scipy (Oliphant (2007)), Millman & Aivazis (2011), Astropy (Pigulski, A. et al. (2001), Astropy Collaboration et al. (2018)) and Pandas (Wes McKinney (2010)).

References

- Angelo, M. S., Santos, J. F. C., Maia, F. F. S., & Corradi, W. J. B. 2022, *Monthly Notices of the Royal Astronomical Society*, 510, 5695
- Astropy Collaboration, Price-Whelan, A. M., Sipőcz, B. M., et al. 2018, *AJ*, 156, 123
- Bayo, A., Rodrigo, C., Barrado Y Navascués, D., et al. 2008, *A&A*, 492, 277
- Bodensteiner, J., Shenar, T., & Sana, H. 2020, *A&A*, 641, A42
- Castelli, F. & Kurucz, R. L. 2003, in *IAU Symposium*, Vol. 210, *Modelling of Stellar Atmospheres*, ed. N. Piskunov, W. W. Weiss, & D. F. Gray, A20
- Cavallo, L., Spina, L., Carraro, G., et al. 2024, *AJ*, 167, 12
- Choi, J., Dotter, A., Conroy, C., et al. 2016, *ApJ*, 823, 102
- Cordoni, G., Casagrande, L., Yu, J., et al. 2024, *MNRAS*, 532, 1547
- de Mink, S. E., Langer, N., Izzard, R. G., Sana, H., & de Koter, A. 2013, *ApJ*, 764, 166
- de Mink, S. E., Sana, H., Langer, N., Izzard, R. G., & Schneider, F. R. N. 2014, *ApJ*, 782, 7
- Dias, W. S., Monteiro, H., Moitinho, A., et al. 2021, *MNRAS*, 504, 356
- Gaia Collaboration. 2022, *Gaia Data Release 3. Summary of the content and survey properties*, *VizieR On-line Data Catalog: I/355*, originally published in: *Astron. Astrophys.*, in prep. (2022)
- Goraya, P. S. 1986, *MNRAS*, 222, 121
- Götzberg, Y., de Mink, S. E., Groh, J. H., et al. 2018, *A&A*, 615, A78
- Granada, A., Jones, C. E., Sigut, T. A. A., et al. 2018, *AJ*, 155, 50
- Hall, J. C. 2008, *Living Reviews in Solar Physics*, 5, 2
- Hunt, E. L. & Reffert, S. 2023, *VizieR Online Data Catalog: Improving the open cluster census. II. (Hunt+, 2023)*, *VizieR On-line Data Catalog: J/A+A/673/A114*. Originally published in: 2023A&A...673A.114H
- Hunter, J. D. 2007, *Computing in Science & Engineering*, 9, 90
- Klement, R., Baade, D., Rivinius, T., et al. 2022, *ApJ*, 940, 86
- Levenhagen, R. S., Diaz, M. P., Coelho, P. R. T., & Hubeny, I. 2017, *ApJS*, 231, 1
- Mathew, B., Subramaniam, A., & Bhatt, B. C. 2008, *MNRAS*, 388, 1879
- Millman, K. J. & Aivazis, M. 2011, *Computing in Science & Engineering*, 13, 9
- Oliphant, T. E. 2007, *Computing in Science & Engineering*, 9, 10
- Pauzen, E., Heiter, U., Netopil, M., & Soubiran, C. 2010, *A&A*, 517, A32
- Peters, G. J. 1976, in *IAU Symposium*, Vol. 70, *Be and Shell Stars*, ed. A. Slettebak, 69
- Peters, G. J., Gies, D. R., Grundstrom, E. D., & McSwain, M. V. 2008, *ApJ*, 686, 1280
- Peters, G. J., Pewett, T. D., Gies, D. R., Touhami, Y. N., & Grundstrom, E. D. 2013, *ApJ*, 765, 2
- Peters, G. J., Wang, L., Gies, D. R., & Grundstrom, E. D. 2016, *ApJ*, 828, 47
- Pigulski, A., Kopacki, G., & Kołaczowski, Z. 2001a, *A&A*, 376, 144
- Pigulski, A., Kopacki, G., & Kołaczowski, Z. 2001b, *VizieR Online Data Catalog: J/A+A/376/144*
- Pigulski, A., Kopacki, G., & Kołaczowski, Z. 2001, *A&A*, 376, 144
- Polis, O. R., Cote, J., Waters, L. B. F. M., & Heise, J. 1991, *A&A*, 241, 419
- Postma, J. E. & Leahy, D. 2017, *PASP*, 129, 115002
- Rani, S., Pandey, G., Subramaniam, A., et al. 2021, *ApJ*, 923, 162
- Rauch, T. & Deetjen, J. L. 2003, in *Astronomical Society of the Pacific Conference Series*, Vol. 288, *Stellar Atmosphere Modeling*, ed. I. Hubeny, D. Mihas, & K. Werner, 103
- Rebassa-Mansergas, A., Solano, E., Jiménez-Esteban, F. M., et al. 2021, *MNRAS*, 506, 5201
- Rivinius, T., Carciofi, A. C., & Martayan, C. 2013, *A&A Rev.*, 21, 69
- Sanduleak, N. 1979, *AJ*, 84, 1319
- Sanduleak, N. 1990, *AJ*, 100, 1239
- Shao, Y. & Li, X.-D. 2014, *ApJ*, 796, 37
- Shao, Y. & Li, X.-D. 2021, *ApJ*, 908, 67
- Stetson, P. B. 1987, *PASP*, 99, 191
- Tandon, S. N., Postma, J., Joseph, P., et al. 2020, *AJ*, 159, 158
- Tandon, S. N., Subramaniam, A., Girish, V., et al. 2017, *AJ*, 154, 128
- Taylor, M. 2011, *TOPCAT: Tool for Operations on Catalogues And Tables*, *Astrophysics Source Code Library*, record ascl:1101.010
- van Bever, J. & Vanbeveren, D. 1997, *A&A*, 322, 116
- van der Walt, S., Colbert, S. C., & Varoquaux, G. 2011, *Computing in Science & Engineering*, 13, 22
- Wang, L., Gies, D. R., Peters, G. J., et al. 2021, *AJ*, 161, 248
- Wes McKinney. 2010, in *Proceedings of the 9th Python in Science Conference*, ed. Stéfan van der Walt & Jarrod Millman, 56 – 61
- Whitford, A. E. 1958, *AJ*, 63, 201
- Yadav, R. K. S. & Sagar, R. 2001, *MNRAS*, 328, 370
- Yu, P. C., Lin, C. C., Chen, W. P., et al. 2015, *AJ*, 149, 43

Appendix A: Colour-Magnitude Diagrams

Hunt & Reffert (2023) presented the PM membership study of 7167 star clusters using Gaia DR3 catalogue (Gaia Collaboration 2022), including NGC 663, and they found 1081 stars as PM members of the cluster with membership probability (P_{PM}) more than 50%. To identify optical counterparts of UVIT detections, we cross-matched the Hunt & Reffert (2023) catalogue ($P_{PM}>50\%$) with sources detected in both FUV and NUV images. The P_{PM} of the 23 Be stars are tabulated in Table B.1.

Figure A.2 shows the optical, FUV-optical, and NUV-optical Colour-Magnitude Diagrams (CMDs) along with overlaid MIST isochrones taken from Choi et al. (2016) generated for both UVIT and Gaia DR3 filters for the cluster parameters (as mentioned in the caption). We used isochrones with a metallicity of $[Fe/H] = -0.125$ dex and $Z = 0.003110$, excluding initial rotation effects. The optical magnitudes were converted from Vega to AB magnitude system using appropriate conversion factors provided in Gaia documentation².

We cross-matched UVIT-detected stars with Be stars catalogued in Yu et al. (2015), identifying 23 stars. Of these, 22 are detected in F148W, F154W, and F169M, 1 in N263M, and 23 in N279N, all with membership probabilities exceeding 50%. All identified Be stars are represented by green triangles, cyan rectangles and blue pentagons in the optical CMD, as illustrated in Figure A.2. A significant spread is observed along the main-sequence (MS), especially at its bright end spanning ~ 0.45 mag in BP–RP colour. The FUV-optical and NUV-optical CMDs also show the spread at the bright end of the MS, but FUV and NUV optical colours span ~ 2 mag larger than optical colour mainly due to the sensitivity of the UV-optical colour to T_{eff} . Also, the turn-off region of NGC 663 appears slightly broadened, partially influenced by the presence of Be stars. Extended main-sequence turn-offs (eMSTOs), likely caused by enhanced stellar rotation, have been observed in OCs with ages between approximately 50 Myr and 2 Gyr (see (Cordoni et al. 2024) and references therein). However, NGC 663 is younger than the typical eMSTO clusters, and the spread at the turn-off appears to be prominent; therefore, this cluster may be the youngest to show the eMSTO phenomenon. As this cluster is known to have a differential reddening, we also adopt an extinction range from $A_V=2.17$ to $A_V=2.9$ in all CMDs.

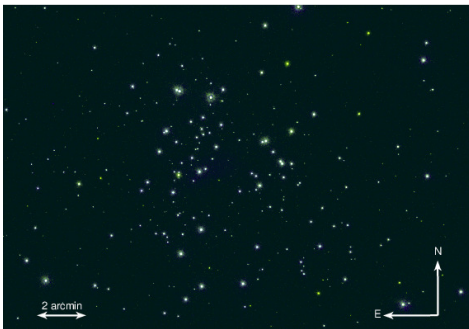
Since the Be stars have a high rotational velocity, their effective temperature (T_{eff}) are affected leading to fast rotators on the red edge of the MS, whereas slow rotators in its blue side. To assess the impact of T_{eff} on UV-optical colour (which is more sensitive to T_{eff}), Colour-Colour Diagrams (CCDs) are constructed using the FUV and NUV filters. The linear plot of (Gbp-Grp) against (F154W-G), (F169M-G), and (N279-G) are shown in Figure A.2. In all CCDs, optical colour (Gbp-Grp) spans a 0.6 mag range, whereas the FUV-G colour spans about 3 mag, a similar trend can be seen in the case of the NUV-G (~ 2.5 mag) colour diagram. We note that some Be stars show bluer UV-optical colour, suggestive of a possible UV excess, as they are bluer in the UV-optical colour.

Table A.1: A log of UVIT observations and different extinction values adopted for NGC 663.

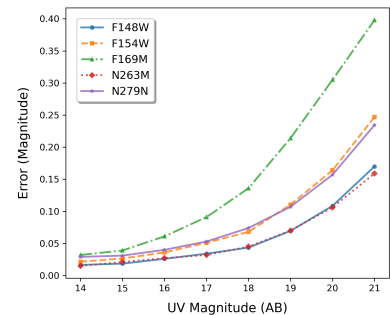
Filter	λ_{mean} (Å)	$\Delta\lambda$ (Å)	ZP (AB mag)	T_{exp} (sec)	A_V	A_{F148W}	A_{F154W}	A_{F169M}	A_{N263M}	A_{N279N}
F148W	1481	500	18.09	1191.673	2.17 ^a	5.794	5.664	5.555	4.579	4.231
F154W	1541	380	17.77	493.823	2.268 ^b	6.056	5.919	5.806	4.785	4.423
F169M	1608	290	17.41	194.791	2.79 ^c	7.449	7.282	7.142	5.887	5.440
N263M	2632	275	18.14	1201.311						
N279N	2792	90	16.50	1412.314						

Notes. The first five columns list filter characteristics and total exposure times. The next six columns present extinction values A_V reported in the literature and the corresponding extinction in UVIT passbands.

References. (a) Granada et al. (2018); (b) Dias et al. (2021); (c) Angelo et al. (2022).



(a) Composite two-colour image of NGC 663: blue (F148W, FUV) and yellow (N279N, NUV).



(b) PSF-fit errors (mean) vs. magnitude for UVIT observations of NGC 663 in three FUV and two NUV bands.

Fig. A.1: (Left) UVIT two-colour image of NGC 663. (Right) PSF-fit magnitude errors.

² <https://www.cosmos.esa.int/web/gaia-users/archive>

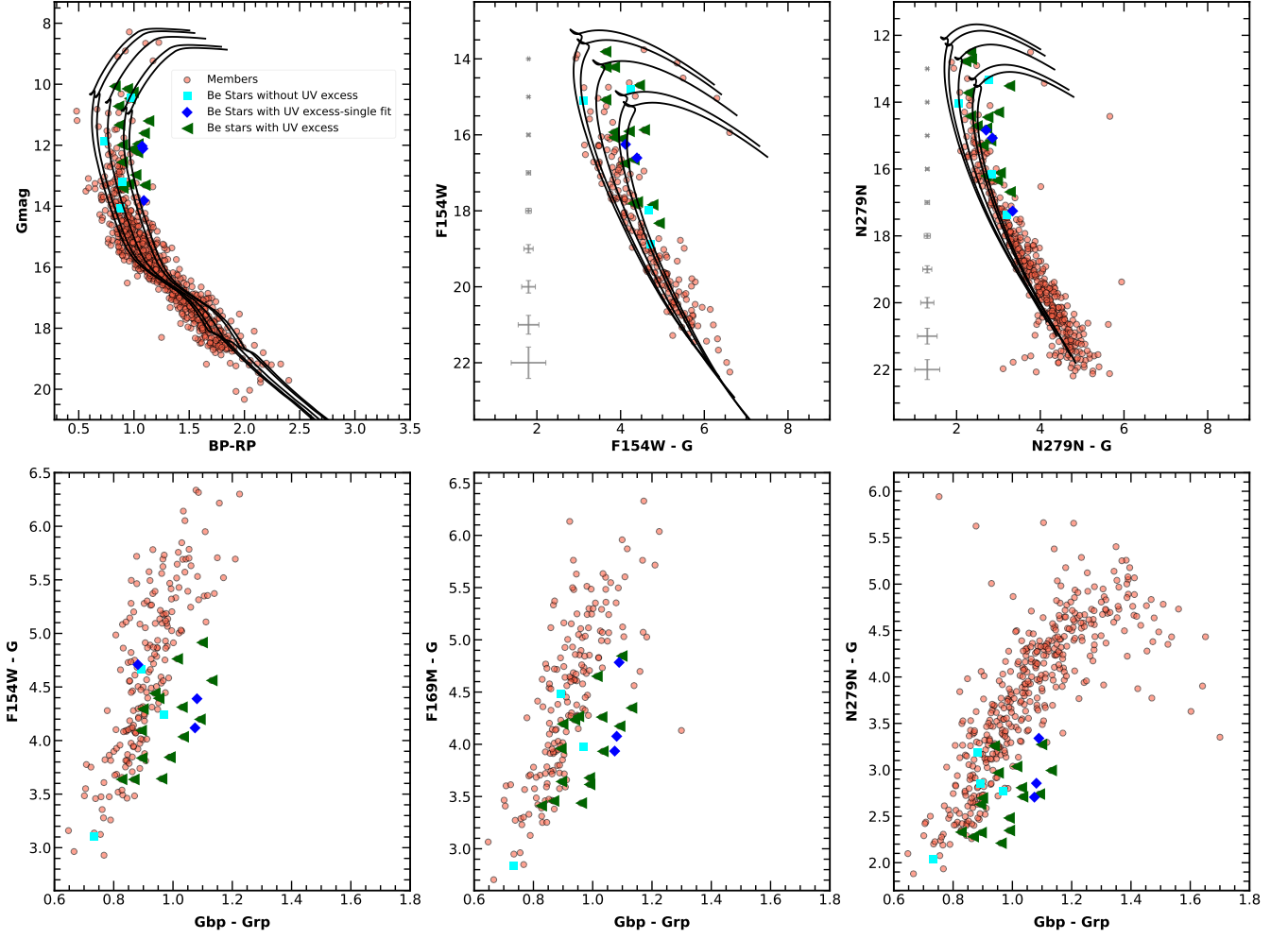


Fig. A.2: Top Panel: The first panel presents the optical CMD of NGC 663, based on Gaia DR3 photometry. Red points represent the optical counterparts (Gaia DR3) of the UVIT FUV/NUV detections. Be stars with UV excess, Be stars without UV excess, and Be stars showing UV excess but not fitted with a double component SED are shown as green triangles, cyan squares, and blue pentagons, respectively. MIST isochrones corresponding to an age of 25 Myr and metallicity $[\text{Fe}/\text{H}] = -0.125$ dex are overplotted as black solid lines for various values of A_V ranging from 2.17 to 2.9 from left to right, assuming a reddening of $E(B-V) = 0.7$ mag and a distance modulus of $(m-M)_V = 11.86$ mag. The second and third panels in the upper panel show the FUV-optical and NUV-optical CMDs created using the F154W and N279N passbands, respectively, for the confirmed members of the cluster. Median error bars are displayed in grey on the left side of FUV and NUV-optical CMDs. Bottom Panel: The first, second, and third panels present CCDs in the FUV-F154W vs. F154W, FUV-F169M vs. F169M, and NUV-N279N vs. N279N planes, respectively. The meaning of the symbols shown is provided in the top-left panel of the first column.

Appendix B: SED fits of Be stars

The details of the SED fitting are elaborated in section 5. The SED fits, single as well as binary, of the rest of the Be stars are shown in Figure B.1

Table B.1: This table presents the fitting parameters for 23 detected Be stars in NGC 663.

Object	RA (Deg)	DEC (Deg)	P_{PM} (%)	Comp.	Model	T_{eff} (K)	L/L_{\odot}	R/R_{\odot}	χ^2_{red}	Vgf	Vgfb	N_{fit}/N_{tot}
D01 034*	26.765589	61.292236	68	–	Kurucz	8750 ± 125	364 ± 69	8.34 ± 0.80	16.6	110	6.0	16/23
GG 109*	26.914015	61.305721	69	–	Kurucz	9000 ± 125	366 ± 77	7.88 ± 0.75	21.4	5.8	0.3	16/23
GG 95	26.443295	61.155804	61	–	Kurucz	25000 ± 500	5255 ± 1075	3.96 ± 0.38	34.5	113	5.0	18/20
L613	26.645269	61.107712	82	–	Kurucz	10750 ± 125	176 ± 36	3.84 ± 0.37	18.2	59.9	6.7	19/24
MWC 698	26.497110	61.212685	90	–	Kurucz	14000 ± 500	5622 ± 1623	12.74 ± 1.21	3.9	53.6	3.9	17/21
PKK 4	26.823006	61.221569	78	–	Kurucz	11250 ± 125	91 ± 17	2.53 ± 0.24	30.3	20.8	1.5	13/16
SAN 28*	26.508623	61.250595	93	–	Kurucz	10250 ± 125	123 ± 23	3.52 ± 0.34	16.9	7.6	0.5	18/21
BG 114	26.558376	61.228851	85	Hot	Kurucz	23000 ± 500	187 ± 35	0.85 ± 0.08	14.4	5.9	0.4	22/22
				Cool	Kurucz	11500 ± 125	313 ± 59	4.43 ± 0.42				
BG 15	26.615303	61.207062	100	Hot	Kurucz	42000 ± 500	4263 ± 812	1.23 ± 0.12	5.9	46.9	3.7	24/24
				Cool	Kurucz	11750 ± 125	3261 ± 621	13.70 ± 1.30				
G32	26.619238	61.230675	53	Hot	TMAP (Grid 3)	90000 ± 5000	1806 ± 344	0.17 ± 0.02	14.7	26	2.1	22/22
				Cool	Kurucz	11500 ± 125	404 ± 77	4.94 ± 0.47				
GC 97	26.483740	61.212574	82	Hot	TMAP (Grid 3)	50000 ± 5000	3881 ± 739	0.81 ± 0.08	4.4	47.4	5.5	24/24
				Cool	Kurucz	10000 ± 125	841 ± 160	9.47 ± 0.90				
GG 101	26.648338	61.227543	85	Hot	Levenhagen	58000 ± 500	573 ± 109	0.45 ± 0.04	16.0	129	11.2	24/24
				Cool	Kurucz	10000 ± 125	424 ± 81	6.69 ± 0.64				
GG 102	26.648041	61.263290	62	Hot	Kurucz	50000 ± 500	3616 ± 688	0.81 ± 0.08	1.7	5.3	0.9	20/20
				Cool	Kurucz	10750 ± 125	3035 ± 579	15.88 ± 1.51				
GG 108	26.861519	61.145599	53	Hot	Kurucz	36000 ± 500	1048 ± 199	0.80 ± 0.08	16.3	130	13.5	24/24
				Cool	Kurucz	11500 ± 125	1123 ± 214	8.23 ± 0.78				
GG 93	26.407560	61.133095	65	Hot	Kurucz	24000 ± 500	466 ± 89	1.19 ± 0.11	13.6	109	8.6	21/21
				Cool	Kurucz	10750 ± 125	532 ± 101	6.45 ± 0.61				
GG 94	26.415096	61.216434	68	Hot	Kurucz	39000 ± 500	704 ± 134	0.56 ± 0.05	8.9	43.9	5.3	24/24
				Cool	Kurucz	11500 ± 125	669 ± 127	6.35 ± 0.60				
MWC 700	26.612782	61.167202	82	Hot	Kurucz	39000 ± 500	4221 ± 804	1.41 ± 0.13	32.0	37.4	3.0	23/23
				Cool	Kurucz	12000 ± 125	3816 ± 727	14.15 ± 1.35				
PKK 2	26.449562	61.273327	62	Hot	Kurucz	35000 ± 500	148 ± 28	0.32 ± 0.03	7.1	64.3	4.3	24/24
				Cool	Kurucz	10500 ± 125	201 ± 38	4.23 ± 0.40				
PKK 3	26.601690	61.177017	95	Hot	Kurucz	25000 ± 500	70 ± 13	0.43 ± 0.04	13.1	30.4	5.5	24/24
				Cool	Kurucz	10250 ± 125	128 ± 24	3.53 ± 0.34				
VES 616	26.525537	61.227573	57	Hot	TMAP (Grid 3)	50000 ± 5000	2984 ± 568	0.70 ± 0.07	4.9	58.6	2.2	21/21
				Cool	Kurucz	12000 ± 125	664 ± 129	7.93 ± 0.75				
VES 619	26.611837	61.128258	91	Hot	TMAP (Grid 3)	50000 ± 5000	8095 ± 1542	1.18 ± 0.11	13.6	171	10.8	24/24
				Cool	Kurucz	10000 ± 125	1749 ± 337	13.80 ± 1.31				
VES 620	26.627619	61.241455	81	Hot	TMAP (Grid 3)	60000 ± 500	1768 ± 336	0.38 ± 0.04	9.8	124	10.7	24/24
				Cool	Kurucz	10000 ± 125	485 ± 92	7.06 ± 0.67				
VES 624	26.748318	61.208199	83	Hot	Kurucz	30000 ± 500	100 ± 19	0.35 ± 0.03	14.7	28.3	5.4	25/25
				Cool	Kurucz	10000 ± 125	151 ± 28	4.00 ± 0.38				

Notes. The upper portion lists stars fitted with a single-component model, while the lower portion includes stars fitted with a two-component model. Column 1 gives the object names used in this work. Columns 2 and 3 provide the RA and DEC of the stars. Column 4 lists the P_{PM} of all Be stars in the cluster. Column 5 indicates the hot or cool component (in the case of a double fit), and column 6 specifies the models used. The effective temperatures T_{eff} , luminosities, and radii of the stars, along with their respective uncertainties, are presented in Columns 7, 8, and 9. Columns 10, 11, 12, and 13 list the χ^2_{red} , Vgf, Vgfb value for the best fit and the ratio of the number of photometric data points used for the fit (N_{fit}/N_{tot}) to the total number of available data points, respectively. Also, objects marked with an asterisk (*) show UV excess but could not be fitted with a binary fit.

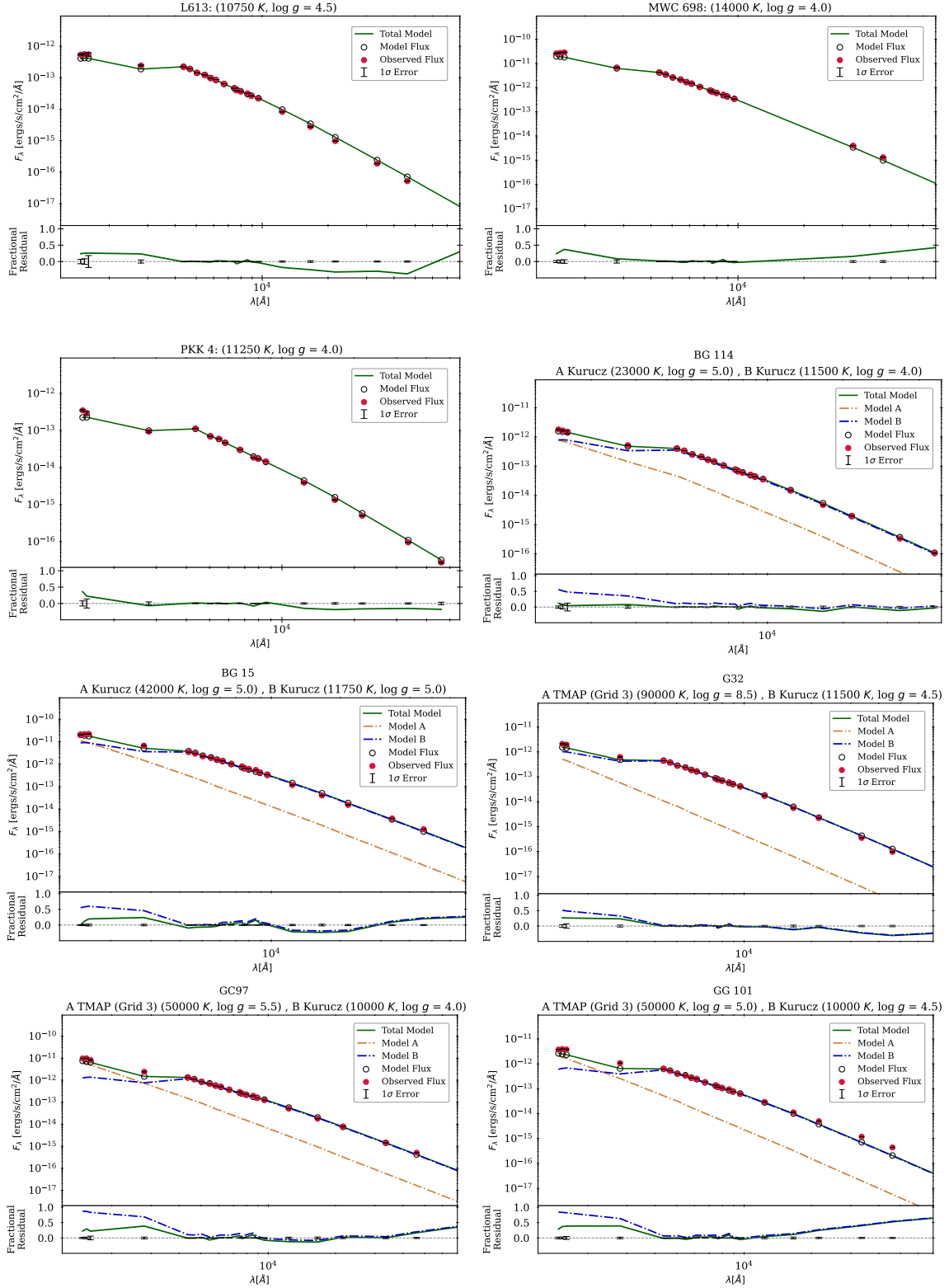


Fig. B.1: Best SED fits, including single and binary model fits, of the rest of the Be stars. The SEDs illustrated in the uppermost panel are of three stars showing no UV excess and fitted well with a single model SED. The symbols and models denote the same as in Figure 1.

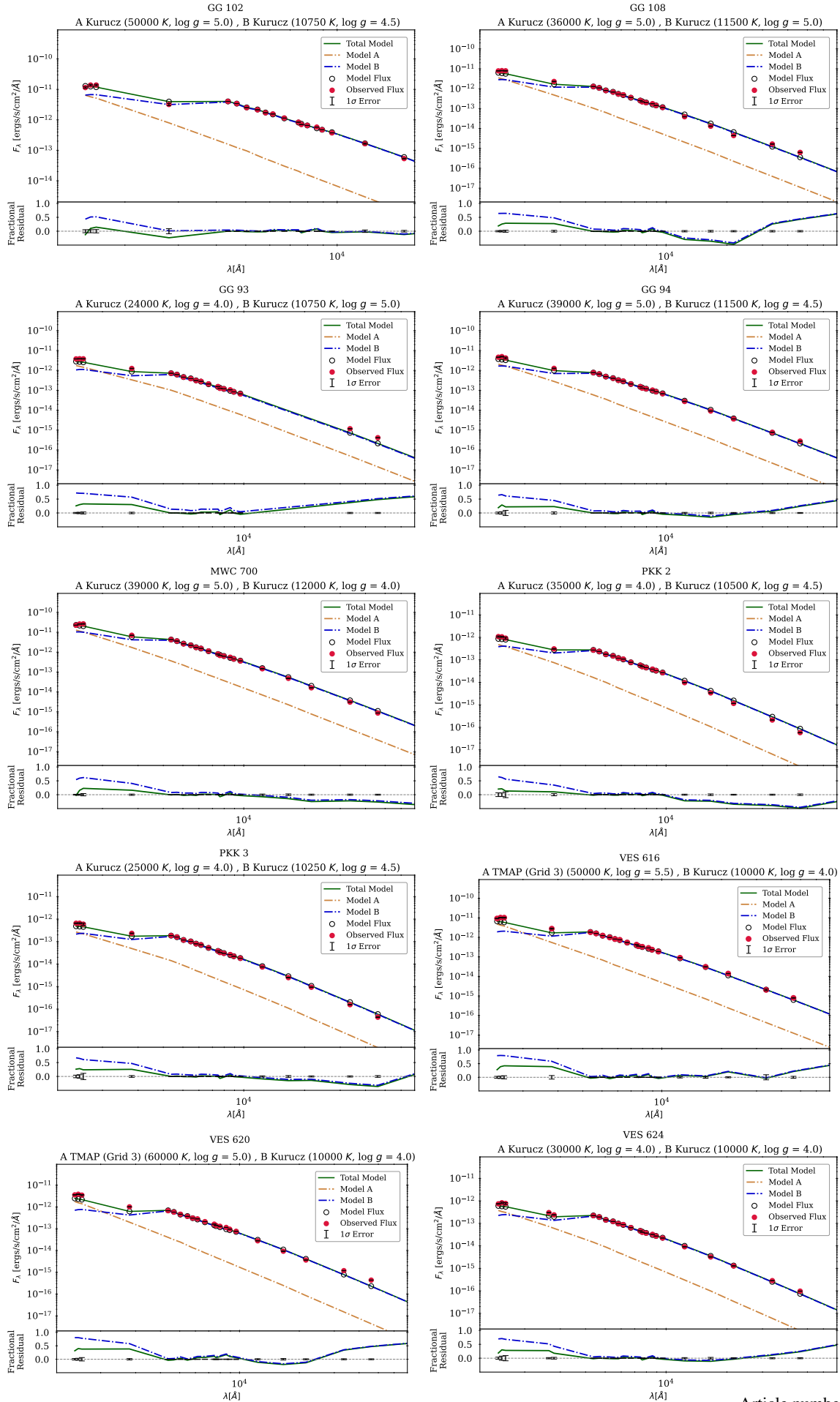


Fig. B.1: continued.